

UC Berkeley

UC Berkeley Previously Published Works

Title

Mechanism of Methanol Decomposition over Single-Site Pt1/CeO2 Catalyst: A DRIFTS Study

Permalink

<https://escholarship.org/uc/item/81v9v6hz>

Journal

Journal of the American Chemical Society, 143(1)

ISSN

0002-7863

Authors

Qi, Zhiyuan
Chen, Luning
Zhang, Shuchen
[et al.](#)

Publication Date

2021-01-13

DOI

10.1021/jacs.0c10728

Peer reviewed

Mechanism of Methanol Decomposition over Single-site Pt₁/CeO₂ Catalyst: a DRIFTS study

Zhiyuan Qi,^{†,#} Luning Chen,^{‡,#} Shuchen Zhang,[‡] Ji Su^{*,‡}, Gabor A. Somorjai^{*,‡,§}

[†]Chemical Sciences Division, [‡]Materials Sciences Division, [‡]Molecular Foundry, Lawrence Berkeley National Laboratory, Berkeley, CA, 94720, United States

[§]Department of Chemistry, University of California-Berkeley, Berkeley, CA, 94720, United States

ABSTRACT: Single-site catalysts have drawn broad attention in catalysis due to the maximum atomic utilization and unique catalytic performance. Early work in our group has shown a 40-fold higher activity of methanol decomposition over single-site Pt₁/CeO₂ catalyst than CeO₂ supported 2.5 nm Pt nanoparticles, while a molecular-level understanding of such enhancement is lacking. Herein, the reaction mechanism of methanol decomposition over Pt₁/CeO₂ was carefully investigated using *in situ* DRIFTS and a reaction pathway was proposed. Methanol molecules were dissociatively adsorbed on nanoceria support first, followed by the diffusion of as-formed methoxy species onto Pt single sites where the dehydrogenation occurs and results in the weakly bonded CO. The ease of methanol dissociative adsorption on nanoceria support and the tailored electronic property of Pt₁ via the metal-support interaction are believed to be strongly correlated with the high activity of Pt₁/CeO₂.

Single-site catalysts (SSCs), with isolated metal sites atomically dispersed on the support, have drawn growing research interests in recent years.¹⁻⁴ Noble metals⁵⁻¹⁰ and transition metals¹¹⁻¹² SSCs over metal oxides¹³, graphene¹⁴⁻¹⁵, heteroatom doped carbon¹⁶⁻¹⁷ have been applied in electrocatalysis¹⁸ and heterogeneous catalysis.¹⁹ Thanks to the flourish of *in situ* and *operando* techniques, the coordination environment and electronic structure of active sites in SSCs could be well characterized, leading to a clearer understanding of their structure-property relationship.²⁰ More recently, mechanistic studies of noble metal SSCs via *in situ* spectroscopy have been reported, while only a few reactions were investigated (e.g., CO oxidation).²¹⁻²³ Therefore, the explored reaction scope needs to be further expanded to better design SSCs.

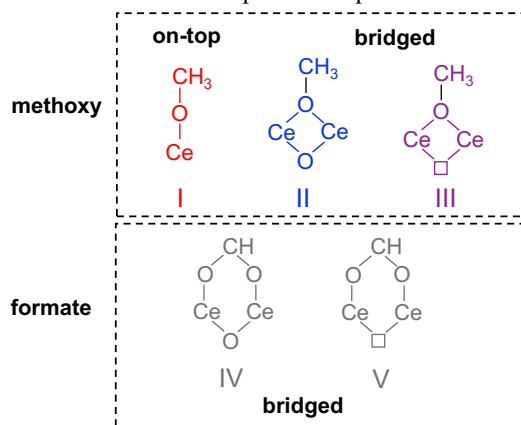
Methanol is an alternative energy source for fossil fuels and important raw material for synthetic chemicals.²⁴ Its convenient production from syngas and renewable biomass allows the wide application in direct methanol fuel cells (DMFCs).²⁵ Besides, methanol could function as a hydrogen carrier to transport hydrogen in the liquid form and release hydrogen via catalytic reactions, taking advantage of its high hydrogen content (12.6 wt.%), easy transportation, and low cost. Our group has demonstrated the potential use of methanol as the liquid organic hydrogen carrier (LOHC), assisted by CeO₂ supported Pt SSCs (denoted as Pt₁/CeO₂).²⁶ Pt₁/CeO₂ with a hydrogen production rate of 12500 h⁻¹ from direct methanol decomposition shows a 40 times higher activity than 2.5 nm Pt/CeO₂. However, a systematic study of the origin of this superior reactivity was not presented. Fortunately, methanol's dehydrogenation mechanism on Pt single crystal²⁷⁻²⁸ and CeO₂ support²⁹⁻³⁰ have been investigated both experimentally and computationally, which builds up a solid foundation for the mechanistic study of methanol decomposition over Pt₁/CeO₂. Herein, we systematically investigated the intermediates of methanol decomposition over

Pt₁/CeO₂, pure CeO₂, and 2.5 nm Pt/CeO₂ using diffuse reflectance infrared Fourier transform spectroscopy (DRIFTS) and proposed a support-assisted reaction mechanism.

Pt₁/CeO₂ was synthesized following the previous report.²⁶ The porous CeO₂ nanorods with 10-15 nm width and 200-300 nm length (Figure S1) were pretreated with ascorbic acid to generate the oxygen vacancies that provide the anchoring sites for Pt atoms. The presence of isolated Pt atoms was confirmed by high-angle annular dark-field transmission electron microscopy (HAADF-STEM), elemental mapping, X-ray absorption near edge structure (XANES), and extended X-ray absorption fine structure (EXAFS)(Figure S2-4, Table S1). DRIFTS spectrum demonstrated only linearly adsorbed CO on Pt^{δ+} sites was observed at 2090 cm⁻¹, further suggesting the single-site feature of Pt atoms (Figure S5). Detailed synthetic methods and characterization data are included and discussed in the supporting information.

DRIFTS spectra of methanol over CeO₂. The methanol adsorption over nanoceria is dissociative, and the formed methoxy could bond with one (on-top), two (bridged), and three (triply bridging) cerium cations.³¹ The ν(CO) stretching vibration in the range of 1000-1100 cm⁻¹ discerns between different methoxy species, which helps to understand the local environment, including oxygen vacancy. Figure 1a shows the temperature-dependent DRIFTS spectra after 10 min methanol vapor dosing min over pure CeO₂ (solid lines, above). At room temperature (Figure S6-S7), the surface was mainly covered by on-top and bridged methoxy (Scheme 1, type I, II, III). The type I methoxy is characterized by the peak set (2912 cm⁻¹(ν_{as}(CH)); 2833 cm⁻¹(ν_s(CH)); 1440 cm⁻¹(δ_{as}(CH), and 1108 cm⁻¹ ν(CO), red dashed trendlines), while another peak set (2924 cm⁻¹(ν_{as}(CH)); 2804 cm⁻¹(ν_s(CH)); 1063 cm⁻¹ ν(CO), blue dashed trendlines) represents the type II methoxy. The shoulder peak at ~1030 cm⁻¹ is assigned to the ν(CO) vibration of methoxy adsorbed on cerium

atoms with a neighboring oxygen vacancy³² (type III, purple dashed trendline). The physisorbed methanol (shoulder peak at $\sim 2941\text{ cm}^{-1}$) and a trace of triply bridging methoxy (shoulder peak at $\sim 1010\text{ cm}^{-1}$) were also detected. These methoxy peak features remained unchanged from room temperature to $150\text{ }^\circ\text{C}$. When above $200\text{ }^\circ\text{C}$, a small redshift in type I $\nu(\text{CO})$ ($\sim 1100\text{ cm}^{-1}$) was observed along with slightly decreased intensity, while bridged $\nu(\text{CO})$ (II and III) has higher overall intensity as temperature increases. Besides methoxy, formate (Scheme 1, IV, V) started to form at $100\text{ }^\circ\text{C}$ and reached a stable intensity at $200\text{ }^\circ\text{C}$, confirmed by the peak set (2933 cm^{-1} ; 2844 cm^{-1} ($\nu(\text{CH})$); 1377 cm^{-1} ($\delta(\text{CH})$), 1580 cm^{-1} $\nu_{\text{as}}(\text{OCO})$ and 1355 cm^{-1} $\nu_{\text{s}}(\text{OCO})$, species IV). Oxygen vacancy also leads to the redshift of $\nu(\text{OCO})$, resulting in two more vibrational modes with lower intensities (1555 cm^{-1} $\nu_{\text{as}}(\text{OCO})$ and 1330 cm^{-1} $\nu_{\text{s}}(\text{OCO})$, species V). Our findings of surface intermediates over nanoceria are consistent with previous reports.³¹⁻³²



Scheme 1. Structures of the surface methoxy and formate on CeO₂ discussed in this work.

Dynamic change of surface methoxy and formate. Similarly, DRIFTS spectra of methanol adsorption over Pt₁/CeO₂ were shown in Figure 1b. The spectra of Pt₁/CeO₂ and CeO₂ measured at $25\text{ }^\circ\text{C}$ were almost identical, while distinctive peak features were observed at elevated temperatures. The type I $\nu(\text{CO})$ has a decreasing intensity along with a graduate redshift above $50\text{ }^\circ\text{C}$, indicating a higher degree of coordinative unsaturation of CeO₂ support with the increasing temperature. Meanwhile, bridged $\nu(\text{CO})$ changed from the coexistence of II and III at lower temperatures to only type III above $200\text{ }^\circ\text{C}$, with an overall increasing intensity. A similar trend was observed in the C-H stretching region ($3100\text{-}2700\text{ cm}^{-1}$): the weak on-top $\nu_{\text{as}}(\text{CH})$ at 2912 cm^{-1} slowly decays as temperature increases, while the bridged $\nu_{\text{as}}(\text{CH})$ at 2926 cm^{-1} becomes clearer, demonstrating the transition from on-top to bridged methoxy at elevated temperature. Therefore, on-top methoxy species are believed to be more reactive, while type III species are more stable at higher temperatures, indicating the neighboring oxygen vacancies could offer the extra stability. Besides, formate was readily formed at $50\text{ }^\circ\text{C}$ with no further increase of intensity at higher temperatures, suggesting Pt single sites could facilitate the conversion of methoxy to formate.

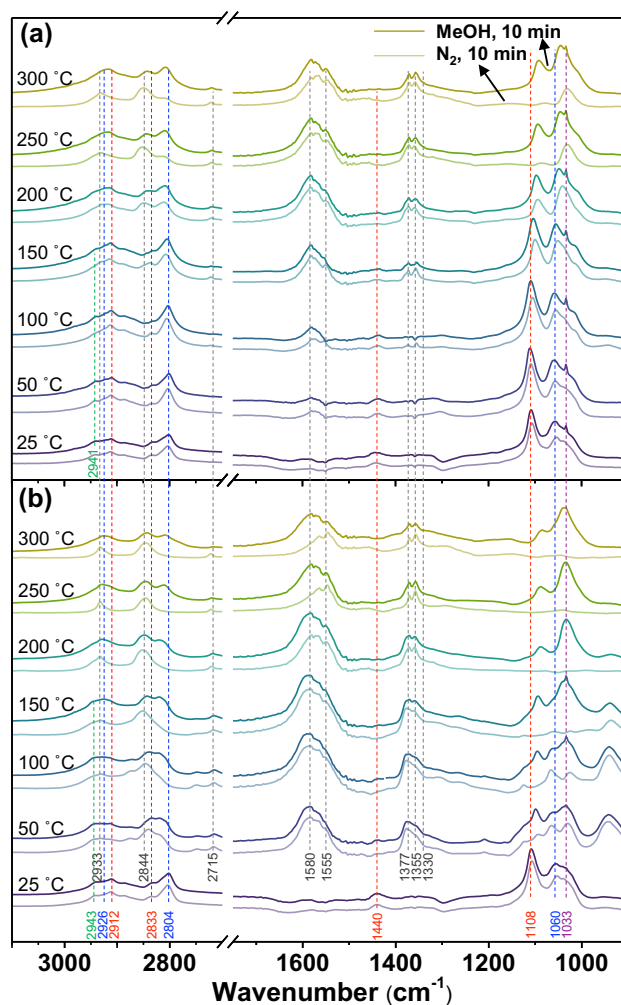


Figure 1. Temperature-dependent DRIFTS spectra of (a) CeO₂ and (b) Pt₁/CeO₂. At each temperature, methanol vapor was first purged for 10 min with N₂ as the carrier gas (solid line, above). Pure N₂ was then purged for another 10 min (faded line, below). The dashed lines in red, blue, purple, and grey were marked for species I, II, III, IV(V), respectively.

After methanol adsorption, pure N₂ was purged for 10 min, and the corresponding DRIFTS spectra were shown as faded lines in Figure 1. The methoxy peaks of Pt₁/CeO₂ starts to decline at $50\text{ }^\circ\text{C}$ and disappears above $150\text{ }^\circ\text{C}$. In contrast, the methoxy over CeO₂ remained their intensity after N₂ purge until $200\text{ }^\circ\text{C}$, above which a slow decay occurs with an order of I, II, and III. Even at $300\text{ }^\circ\text{C}$, there are still $\sim 23\%$ of III and 3.3% of I left on CeO₂. Therefore, we could conclude the disappearance of methoxy over Pt₁/CeO₂ (especially at lower temperatures) is mostly via the reaction instead of desorption. At the same time, formate species on CeO₂ maintained the peak intensity at all temperatures while a slight peak intensity change over Pt₁/CeO₂ could only be observed above $250\text{ }^\circ\text{C}$, indicating the stronger adsorption and much lower activity of formate than methoxy.

Figure 2 represents the time evolution of methoxy intermediates during N₂ purge over different catalysts at $250\text{ }^\circ\text{C}$, starting from the adsorption steady-state (0 min). Type I and III over Pt₁/CeO₂ quickly vanished in 3 min, while 25% of III remained at 10 min on CeO₂, confirming the single-site Pt is the active site. Besides, in both Pt₁/CeO₂ and CeO₂, type I $\nu(\text{CO})$ fades more rapidly than type III $\nu(\text{CO})$ (Figure 2a, 2b insets), showing the higher

activity of on-top methoxy. Figure 2c shows a three-fold intensity of bridged methoxy (type II) over 2.5 nm Pt/CeO₂, indicating methoxy is also largely adsorbed on the surfaces of Pt NPs. Interestingly, the peak height of I and II on 2.5 nm Pt/CeO₂ has no significant change after 2 min, revealing the stronger methoxy adsorption on Pt surface than CeO₂ support and the lower activity of Pt NPs compared to single-site Pt atoms. Previous report showed the methanol decomposition preferentially occurred at the interface between Pt and CeO₂ NPs.³³ Different from 2.5 nm Pt/CeO₂ where only a small number of Pt atoms interface with CeO₂ support, every Pt atom in Pt₁/CeO₂ has the direct interaction with CeO₂, which not only maximize the Pt utilization efficiency but also enhance the specific activity of each active site. Therefore, the superior activity of Pt₁/CeO₂ is suggested to be a result of the strong interaction between single-site Pt and CeO₂ support. In all three cases, the formate species were stable on the surface, with a relatively identical intensity over time (Figure S8).

The effect of CeO₂ support in single-site catalysis. To further explore the metal-support interaction, we prepared Pt SSCs with two other supports, namely Pt₁/Al₂O₃ and Pt₁/TiO₂. CO DRIFTS confirmed the single-site feature in both catalysts (Figure S9). However, these two Pt SSCs only showed trace methanol conversion (<0.1%) at 300 °C (Figure S10), demonstrating

the critical role played by CeO₂. Methanol DRIFTS (Figure S11) showed that methoxy could desorb at room temperature on both Pt₁/Al₂O₃ and Pt₁/TiO₂, probably because the dissociative adsorption is not highly preferred on these two supports.^{34,35} The easy desorption of surface species makes it difficult for reactants to access the Pt single sites, thus leading to lower activity. Commercial CeO₂ supported Pt SSC was also prepared and compared (denoted as Pt₁/commercial CeO₂). Due to the low surface area of this bulk support, the adsorbed surface methoxy amount is much lower (Figure S12). However, Pt₁/commercial CeO₂ obtained a similar TOF at 300 °C compared to Pt₁/CeO₂ (Table S2), further confirming the activity is from the interaction between single-site Pt and CeO₂. We thus believed the dissociative adsorption of methanol on nanoceria is the critical step for methanol decomposition over supported Pt SSCs. Besides, the presence of oxygen vacancy could also enhance the methanol adsorption (Figure S13) and stabilize the formed methoxy species (the dominant type III in Figure 1). It has been proposed that one isolated Pt atom (replacing one Ce atom) would create two oxygen vacancies.³⁶ Therefore, the preferential adsorption of methoxy near oxygen vacancy helps to get a higher chance to access single-site Pt. A detailed study of engineering oxygen vacancy is currently on the way.

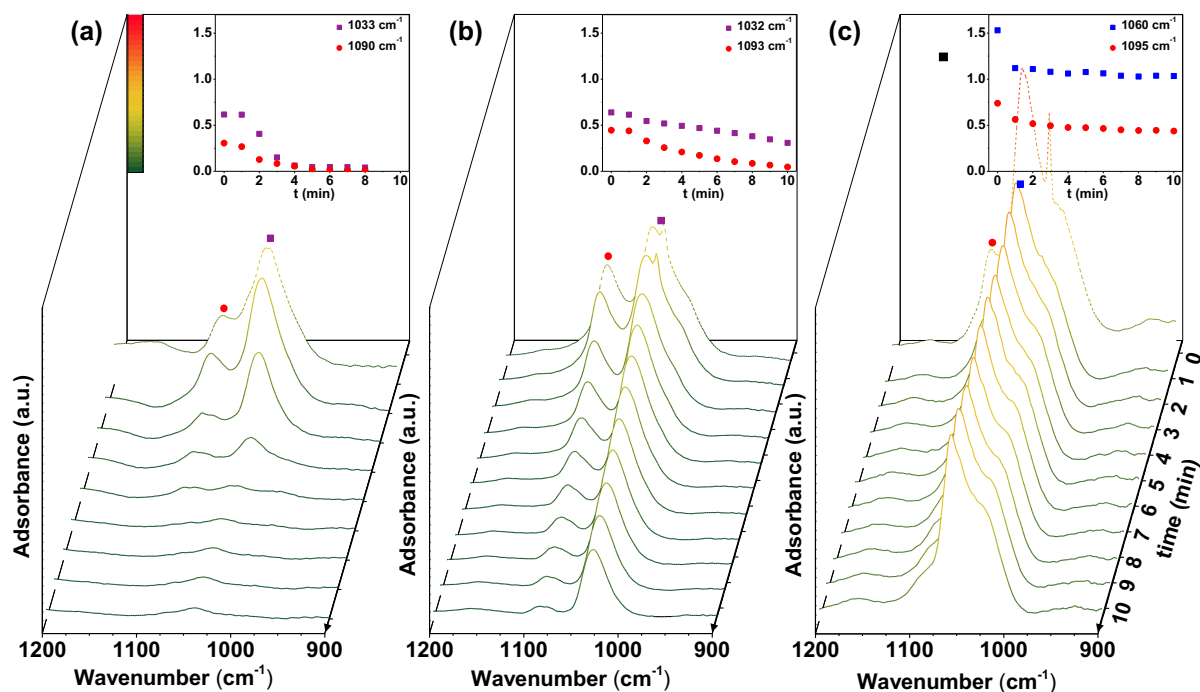


Figure 2. DRIFTS spectra of (a) Pt₁/CeO₂, (b) CeO₂; (c) 2.5 nm Pt NPs/CeO₂ during the N₂ purge at 250 °C. The insets are the peak height change of bridged (II or III) and on-top methoxy (I). Spectra at steady-state were shown as 0 min for reference (dashed line).

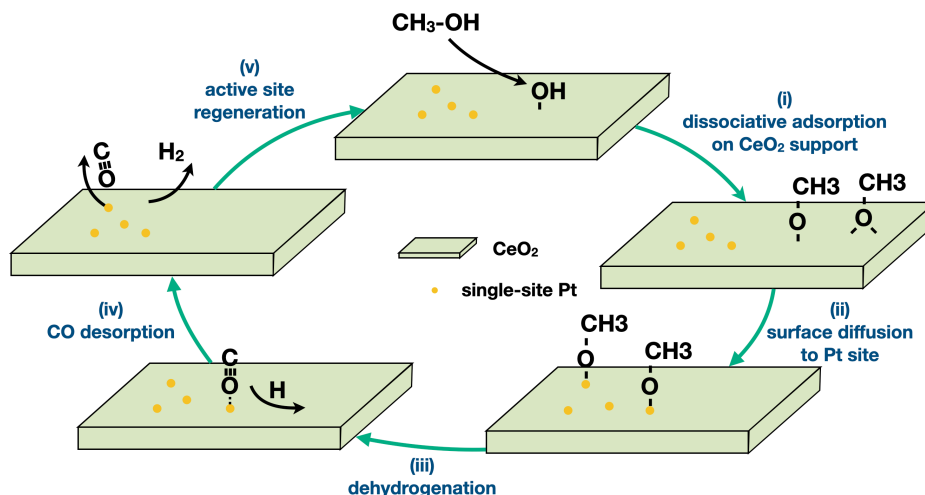


Figure 3. Schematic presentation of the proposed reaction mechanism over Pt₁/CeO₂. The green plate and orange dot represent the CeO₂ support and single-site Pt, respectively.

Based on the above observations, we proposed a reaction pathway of methanol decomposition over Pt₁/CeO₂ (Figure 3). Due to the low surface density of Pt atoms, methanol molecules first react with the lattice oxygen and/or surface hydroxyl of CeO₂ support to form both on-top and bridged methoxy species. Since CeO₂ support showed almost no activity for methanol decomposition, the methoxy species have to diffuse onto Pt atoms for further reactions, with on-top methoxy more active than bridged methoxy. The methoxy species were then dehydrogenated to carbon monoxide on top of single-site Pt above 150 °C, confirmed by both gas chromatography analysis (Table S2) and DRIFTS spectra (Figure S14). The hydrogen atoms then migrated back to the CeO₂ surface and generated the molecular H₂, evidenced by the color change of catalyst after DRIFTS (Figure S15). Finally, the desorption of CO releases the Pt active site, which could be used for the continuous reaction.

In summary, we investigated the reaction intermediates during the methanol decomposition over Pt₁/CeO₂ under various temperatures. DRIFTS spectra reveal easy and strong adsorption of methanol on nanoceria, which is believed to be a prerequisite for methanol decomposition over single-site catalysts. Furthermore, the strong interaction between single-site Pt and CeO₂, along with the easy desorption of carbon monoxide are both contributing to the higher activity of Pt₁/CeO₂ compared to CeO₂ supported Pt NPs. This work exemplifies a DRIFTS study of reaction mechanism over SSCs, and highlights the important role of the catalyst supports, especially on reactant adsorptions. We hope this could provide more guidance in the design of SSCs to tune the reaction pathway and optimize the catalytic performance.

ASSOCIATED CONTENT

Supporting Information

The Supporting Information is available free of charge on the ACS Publications website. Experimental details, characterization of catalysts, DRIFTS spectra of control samples.

AUTHOR INFORMATION

Corresponding Author

Ji Su – Materials Sciences Division and Molecular Foundry, Lawrence Berkeley National Laboratory, Berkeley, California 94720.

Gabor A. Somorjai – Department of Chemistry, University of California-Berkeley, Berkeley, CA, 94720.

Author Contributions

#Z.Q. and L.C. contributed equally to this work.

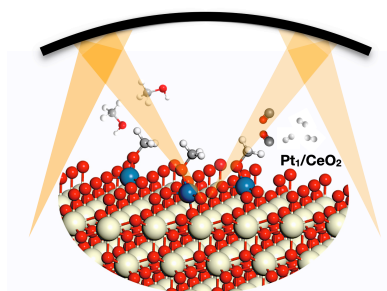
ACKNOWLEDGMENT

This work was supported by Director, Office of Basic Energy Sciences, Division of Chemical Sciences, Geological and Biosciences of the U.S. Department of Energy under contract no. DE-AC02-05CH11231. We thank Jeng-Lung Chen and Chih-Wen Pao at the National Synchrotron Radiation Research Center in Taiwan for the assistance on XAS measurement and EXAFS fitting.

REFERENCES

- Wang, A. Q.; Li, J.; Zhang, T., Heterogeneous single-atom catalysis. *Nat. Rev. Chem.* **2018**, *2* (6), 65-81.
- Cui, X. J.; Li, W.; Ryabchuk, P.; Junge, K.; Beller, M., Bridging homogeneous and heterogeneous catalysis by heterogeneous single-metal-site catalysts. *Nat. Catal.* **2018**, *1* (6), 385-397.
- Chen, Y. J.; Ji, S. F.; Chen, C.; Peng, Q.; Wang, D. S.; Li, Y. D., Single-Atom Catalysts: Synthetic Strategies and Electrochemical Applications. *Joule* **2018**, *2* (7), 1242-1264.
- Yang, X. F.; Wang, A. Q.; Qiao, B. T.; Li, J.; Liu, J. Y.; Zhang, T., Single-Atom Catalysts: A New Frontier in Heterogeneous Catalysis. *Accounts Chem. Res.* **2013**, *46* (8), 1740-1748.
- Lang, R.; Li, T. B.; Matsumura, D.; Miao, S.; Ren, Y. J.; Cui, Y. T.; Tan, Y.; Qiao, B. T.; Li, L.; Wang, A. Q.; Wang, X. D.; Zhang, T., Hydroformylation of Olefins by a Rhodium Single-Atom Catalyst with Activity Comparable to RhCl(PPh₃)₃. *Angew. Chem.-Int. Edit.* **2016**, *55* (52), 16054-16058.
- Lin, L. L.; Zhou, W.; Gao, R.; Yao, S. Y.; Zhang, X.; Xu, W. Q.; Zheng, S. J.; Jiang, Z.; Yu, Q. L.; Li, Y. W.; Shi, C.; Wen, X. D.; Ma, D., Low-temperature hydrogen production from water and methanol using Pt/alpha-MoC catalysts. *Nature* **2017**, *544* (7648), 80-+.
- Pei, G. X.; Liu, X. Y.; Wang, A. Q.; Lee, A. F.; Isaacs, M. A.; Li, L.; Pan, X. L.; Yang, X. F.; Wang, X. D.; Tai, Z. J.; Wilson,

- K.; Zhang, T., Ag Alloyed Pd Single-Atom Catalysts for Efficient Selective Hydrogenation of Acetylene to Ethylene in Excess Ethylene. *ACS Catal.* **2015**, *5* (6), 3717-3725.
8. Qiao, B. T.; Liu, J. X.; Wang, Y. G.; Lin, Q. Q.; Liu, X. Y.; Wang, A. Q.; Li, J.; Zhang, T.; Liu, J. Y., Highly Efficient Catalysis of Preferential Oxidation of CO in H₂-Rich Stream by Gold Single-Atom Catalysts. *ACS Catal.* **2015**, *5* (11), 6249-6254.
9. Tao, H. C.; Choi, C.; Ding, L. X.; Jiang, Z.; Hang, Z. S.; Jia, M. W.; Fan, Q.; Gao, Y. N.; Wang, H. H.; Robertson, A. W.; Hong, S.; Jung, Y. S.; Liu, S. Z.; Sun, Z. Y., Nitrogen Fixation by Ru Single-Atom Electrocatalytic Reduction. *Chem* **2019**, *5* (1), 204-214.
10. Yan, H.; Cheng, H.; Yi, H.; Lin, Y.; Yao, T.; Wang, C. L.; Li, J. J.; Wei, S. Q.; Lu, J. L., Single-Atom Pd-1/Graphene Catalyst Achieved by Atomic Layer Deposition: Remarkable Performance in Selective Hydrogenation of 1,3-Butadiene. *J. Am. Chem. Soc.* **2015**, *137* (33), 10484-10487.
11. Chen, Y. J.; Ji, S. F.; Wang, Y. G.; Dong, J. C.; Chen, W. X.; Li, Z.; Shen, R. A.; Zheng, L. R.; Zhuang, Z. B.; Wang, D. S.; Li, Y. D., Isolated Single Iron Atoms Anchored on N-Doped Porous Carbon as an Efficient Electrocatalyst for the Oxygen Reduction Reaction. *Angew. Chem.-Int. Edit.* **2017**, *56* (24), 6937-6941.
12. Yin, P. Q.; Yao, T.; Wu, Y.; Zheng, L. R.; Lin, Y.; Liu, W.; Ju, H. X.; Zhu, J. F.; Hong, X.; Deng, Z. X.; Zhou, G.; Wei, S. Q.; Li, Y. D., Single Cobalt Atoms with Precise N-Coordination as Superior Oxygen Reduction Reaction Catalysts. *Angew. Chem.-Int. Edit.* **2016**, *55* (36), 10800-10805.
13. Wan, J. W.; Chen, W. X.; Jia, C. Y.; Zheng, L. R.; Dong, J. C.; Zheng, X. S.; Wang, Y.; Yan, W. S.; Chen, C.; Peng, Q.; Wang, D. S.; Li, Y. D., Defect Effects on TiO₂ Nanosheets: Stabilizing Single Atomic Site Au and Promoting Catalytic Properties. *Adv. Mater.* **2018**, *30* (11), 8.
14. Sun, S. H.; Zhang, G. X.; Gauquelin, N.; Chen, N.; Zhou, J. G.; Yang, S. L.; Chen, W. F.; Meng, X. B.; Geng, D. S.; Banis, M. N.; Li, R. Y.; Ye, S. Y.; Knights, S.; Botton, G. A.; Sham, T. K.; Sun, X. L., Single-atom Catalysis Using Pt/Graphene Achieved through Atomic Layer Deposition. *Sci Rep* **2013**, *3*, 9.
15. Deng, D. H.; Chen, X. Q.; Yu, L.; Wu, X.; Liu, Q. F.; Liu, Y.; Yang, H. X.; Tian, H. F.; Hu, Y. F.; Du, P. P.; Si, R.; Wang, J. H.; Cui, X. J.; Li, H. B.; Xiao, J. P.; Xu, T.; Deng, J.; Yang, F.; Duchesne, P. N.; Zhang, P.; Zhou, J. G.; Sun, L. T.; Li, J. Q.; Pan, X. L.; Bao, X. H., A single iron site confined in a graphene matrix for the catalytic oxidation of benzene at room temperature. *Sci. Adv.* **2015**, *1* (11), 9.
16. Zheng, Y.; Jiao, Y.; Li, L. H.; Xing, T.; Chen, Y.; Jaroniec, M.; Qiao, S. Z., Toward Design of Synergistically Active Carbon-Based Catalysts for Electrocatalytic Hydrogen Evolution. *ACS Nano* **2014**, *8* (5), 5290-5296.
17. Fei, H. L.; Dong, J. C.; Arellano-Jimenez, M. J.; Ye, G. L.; Kim, N. D.; Samuel, E. L. G.; Peng, Z. W.; Zhu, Z.; Qin, F.; Bao, J. M.; Yacaman, M. J.; Ajayan, P. M.; Chen, D. L.; Tour, J. M., Atomic cobalt on nitrogen-doped graphene for hydrogen generation. *Nat. Commun.* **2015**, *6*, 8.
18. Xu, H. X.; Cheng, D. J.; Cao, D. P.; Zeng, X. C., A universal principle for a rational design of single-atom electrocatalysts. *Nat. Catal.* **2018**, *1* (5), 339-348.
19. Wang, A.; Li, J.; Zhang, T., Heterogeneous single-atom catalysis. *Nature Reviews Chemistry* **2018**, *2* (6), 65-81.
20. Li, X.; Yang, X.; Zhang, J.; Huang, Y.; Liu, B., In Situ/Operando Techniques for Characterization of Single-Atom Catalysts. *ACS Catalysis* **2019**, *9* (3), 2521-2531.
21. Ding, K.; Gulec, A.; Johnson, A. M.; Schweitzer, N. M.; Stucky, G. D.; Marks, L. D.; Stair, P. C., Identification of active sites in CO oxidation and water-gas shift over supported Pt catalysts. *Science* **2015**, *350* (6257), 189-192.
22. Qiao, B. T.; Wang, A. Q.; Yang, X. F.; Allard, L. F.; Jiang, Z.; Cui, Y. T.; Liu, J. Y.; Li, J.; Zhang, T., Single-atom catalysis of CO oxidation using Pt-1/FeOx. *Nat. Chem.* **2011**, *3* (8), 634-641.
23. Nie, L.; Mei, D. H.; Xiong, H. F.; Peng, B.; Ren, Z. B.; Hernandez, X. I. P.; DeLariva, A.; Wang, M.; Engelhard, M. H.; Kovarik, L.; Datye, A. K.; Wang, Y., Activation of surface lattice oxygen in single-atom Pt/CeO₂ for low-temperature CO oxidation. *Science* **2017**, *358* (6369), 1419.
24. Olah, G. A., Beyond Oil and Gas: The Methanol Economy. *Angewandte Chemie International Edition* **2005**, *44* (18), 2636-2639.
25. Kreuer, K. D., On the development of proton conducting polymer membranes for hydrogen and methanol fuel cells. *J. Membr. Sci.* **2001**, *185* (1), 29-39.
26. Chen, L. N.; Hou, K. P.; Liu, Y. S.; Qi, Z. Y.; Zheng, Q.; Lu, Y. H.; Chen, J. Y.; Chen, J. L.; Pao, C. W.; Wang, S. B.; Li, Y. B.; Xie, S. H.; Liu, F. D.; Prendergast, D.; Klebanoff, L. E.; Stavila, V.; Allendorf, M. D.; Guo, J. H.; Zheng, L. S.; Su, J.; Somorjai, G. A., Efficient Hydrogen Production from Methanol Using a Single-Site Pt-1/CeO₂ Catalyst. *J Am Chem Soc* **2019**, *141* (45), 17995-17999.
27. Gibson, K. D.; Dubois, L. H., Step effects in the thermal decomposition of methanol on Pt(111). *Surface Science* **1990**, *233* (1), 59-64.
28. Greeley, J.; Mavrikakis, M., A First-Principles Study of Methanol Decomposition on Pt(111). *J. Am. Chem. Soc.* **2002**, *124* (24), 7193-7201.
29. Lustemberg, P. G.; Bosco, M. V.; Bonivardi, A.; Busnengo, H. F.; Ganduglia-Pirovano, M. V., Insights into the Nature of Formate Species in the Decomposition and Reaction of Methanol over Cerium Oxide Surfaces: A Combined Infrared Spectroscopy and Density Functional Theory Study. *The Journal of Physical Chemistry C* **2015**, *119* (37), 21452-21464.
30. Araiza, D. G.; Gómez-Cortés, A.; Díaz, G., Reactivity of methanol over copper supported on well-shaped CeO₂: a TPD-DRIFTS study. *Catalysis Science & Technology* **2017**, *7* (22), 5224-5235.
31. Binet, C.; Daturi, M.; Lavalley, J.-C., IR study of polycrystalline ceria properties in oxidised and reduced states. *Catalysis Today* **1999**, *50* (2), 207-225.
32. Rousseau, S.; Marie, O.; Bazin, P.; Daturi, M.; Verdier, S.; Harlé, V., Investigation of Methanol Oxidation over Au/Catalysts Using Operando IR Spectroscopy: Determination of the Active Sites, Intermediate/Spectator Species, and Reaction Mechanism. *J Am Chem Soc* **2010**, *132* (31), 10832-10841.
33. Yamada, Y.; Tsung, C.-K.; Huang, W.; Huo, Z.; Habas, S. E.; Soejima, T.; Aliaga, C. E.; Somorjai, G. A.; Yang, P., Nanocrystal bilayer for tandem catalysis. *Nat. Chem.* **2011**, *3* (5), 372-376.
34. Yang, D.; Li, Y.; Liu, X.; Cao, Y.; Gao, Y.; Shen, Y.R.; Liu, W.-T., Facet-specific interaction between methanol and TiO₂ probed by sum-frequency vibrational spectroscopy. *PNAS* **2018**, *115* (17), E3888-E3894.
35. Busca, G.; Rossi, P.F.; Lorenzelli, V.; Benaissa, M.; Travert, J.; Lavalley, J. C. Microcalorimetric and Fourier transform infrared spectroscopic studies of methanol adsorption on alumina. *J. Phys. Chem.* **1985**, *89*(25), 5433-5439.
36. Liu, C.; Chen, Z.; Yan, H.; Xi, S.; Yam, K.; Gao, J.; Du, Y.; Li, J.; Zhao, X.; Xie, K.; Xu, H.; Li, X.; Leng, K.; Pennycook, J.; Liu, B.; Zhang, C.; Koh, M.-J.; Loh, K.-P. Expedient synthesis of E-hydrazone esters and IH-indazole scaffolds through heterogeneous single-atom platinum catalysis. *Sci. Adv.* **2019**, *5*(12), eaay1537.



Probing Reaction Mechanism on
Single-site Catalysts
